ANNUAL REVIEWS

Annual Review of Biomedical Engineering

Skin-Mountable Biosensors and Therapeutics: A Review

Eun Kwang Lee,[1,*] Min Ku Kim,[1,*] and Chi Hwan Lee[1,2,3]

[1]Weldon School of Biomedical Engineering, Purdue University, West Lafayette, Indiana 47907, USA; email: lee2270@purdue.edu

[2]School of Mechanical Engineering, Purdue University, West Lafayette, Indiana 47907, USA

[3]Department of Speech, Language, and Hearing Sciences, Purdue University, West Lafayette, Indiana 47907, USA

Annu. Rev. Biomed. Eng. 2019. 21:299–323

First published as a Review in Advance on March 18, 2019

The *Annual Review of Biomedical Engineering* is online at bioeng.annualreviews.org

https://doi.org/10.1146/annurev-bioeng-060418-052315

*These authors contributed equally to this article

Keywords

skin-mountable biomedical devices, flexible electronics, biosensors, therapeutics, health monitoring and management, soft packaging

Abstract

Miniaturization of electronic components and advances in flexible and stretchable materials have stimulated the development of wearable health care systems that can reflect and monitor personal health status by health care professionals. New skin-mountable devices that offer seamless contact onto the human skin, even under large deformations by natural motions of the wearer, provide a route for both high-fidelity monitoring and patient-controlled therapy. This article provides an overview of several important aspects of skin-mountable devices and their applications in many medical settings and clinical practices. We comprehensively describe various transdermal sensors and therapeutic systems that are capable of detecting physical, electrophysiological, and electrochemical responses and/or providing electrical and thermal therapies and drug delivery services, and we discuss the current challenges, opportunities, and future perspectives in the field. Finally, we present ways to protect the embedded electronic components of skin-mountable devices from the environment by use of mechanically soft packaging materials.

Contents

1. INTRODUCTION

Continual increases in medical costs arising from the aging population and a rise in chronic diseases have motivated the development of wearable biomedical devices, as such devices allow noninvasive diagnosis of health conditions and provide point-of-care services at home, thereby potentially reducing primary care patient load (1–6). Wearable biomedical devices typically contain arrays of sensors and stimulators, data acquisition systems, and units of wireless powering and data communication that allow accurate detection of physical, electrophysiological, and electrochemical biosignals and/or transfer of therapeutic stimulations or drug molecules to and from the human body (7, 8). These devices exist in many different forms, exploiting wristbands, gloves, socks, and adhesive patches (9, 10). Recent advances in soft functional materials and assembly techniques have enabled the development of mechanically flexible and stretchable devices that can be directly integrated into the human skin in a manner that complies with the natural motion of the wearer (11, 12). The mechanical compliance of such skin-mountable devices allows conformal, seamless skin contact, which plays a critical role in achieving high-fidelity recording of biological signals and efficient therapy during prolonged use in many clinical applications (13). This article reviews recent developments and challenges in the use of skin-mountable devices in various biomedical settings. It also discusses examples of miniaturized units for wireless powering and data communication, as well as soft packaging materials often used for skin-mountable devices.

1.1. Basic Structure of Human Skin

Human skin is not only the largest sensory organ but also one of the best indicators of health condition. Skin thickness varies widely, ranging from 0.04 mm (eyelid) to 1.6 mm (palm); the typical thickness of adult skin is 0.05–0.1 mm (14). Human skin consists of epidermal, dermal, and subcutaneous layers, all connected by a complex vascular nervous network (**Figure 1**). The epidermis (0.4–1.5 mm in thickness) is composed mainly of keratinocytes and is renewed constantly. It can serve as a primary barrier; for instance, the outermost layer of the epidermis protects against mechanical stimulation, prevents evaporation of water from cells, and maintains thermal homeostasis. The dermis, which is more than five times thicker than the epidermis, is the middle layer of skin

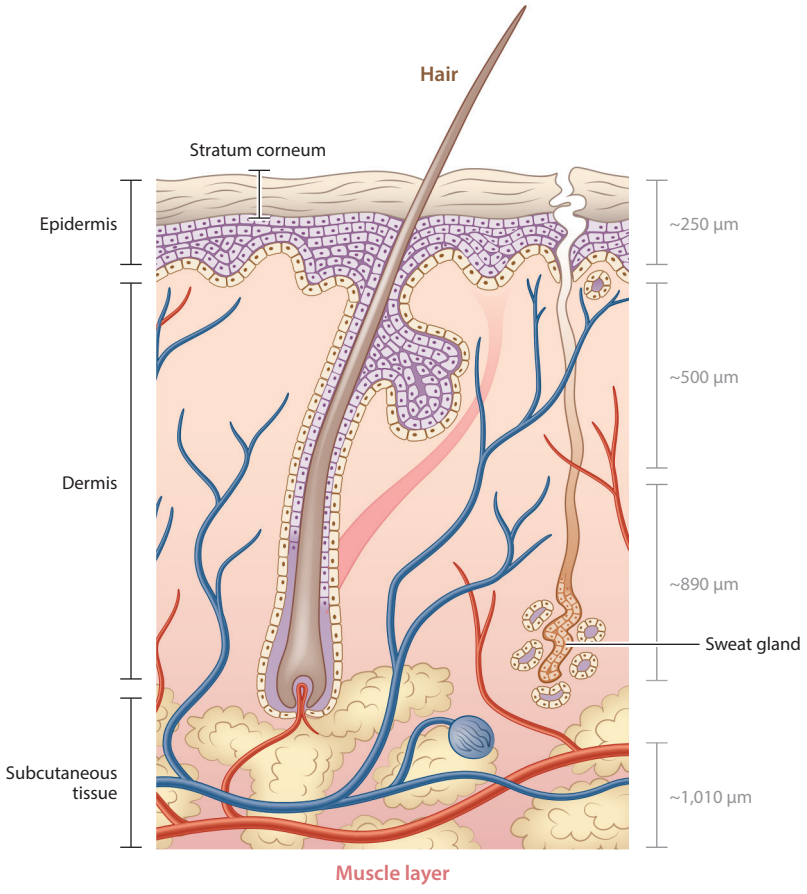

Figure 1

Structure of typical human skin. The main layers are the epidermis and the dermis. Their thickness is typically ~1,640 μm. Adapted with permission from Reference 12.

and is composed of fibroblasts that secrete collagen fibers. Most of the collagen fibers found in the dermis provide the skin with its tensile strength and mechanical resistance. The many blood vessels in the dermis can regulate heat loss through contraction and expansion (15). When blood vessels in the dermis expand, the amount of blood flow increases and the skin becomes warm, allowing excessive heat to be released. Conversely, when the blood vessels contract, blood flow is reduced, resulting in paleness, a feeling of cold, sweating, and heat loss (16). Heat conduction occurs through the dermis and epidermis as a result of blood perfusion under the subcutaneous layer; the average skin temperature depends more on the blood perfusion rate and arterial blood temperature than on the thickness and thermal conductivity of the epidermis and dermis (17, 18). Special sensory receptors in the dermis, known as Pacinian corpuscles, are responsible for sensing cold, heat, pain, and pressure. The subcutaneous layer of the human skin is composed of connective tissues, fat, and large blood vessels. The thickness of the subcutaneous layer varies by person. The subcutaneous tissue acts as a mechanical buffer to protect the skin from external forces and to preserve constant body temperature, and it is actively involved in general energy metabolism and storage (12).

Table 1 Comparison of the physiological parameters of human sweat and human tears

Parameter	Sweat (reference)	Tears (reference)
Daily production, adult	10–14 L/day (141)	160–310 mL/day (142)
Na^+ concentration, adult	10–90 mM (143)	120–165 mM (144)
K^+ concentration, adult	2–10 mM (143)	20–42 mM (144)
Cl^- concentration, adult	118–135 mM (145)	106–135 mM (146)
pH	4.5–7.0 (137)	6.5–7.6 (147)
Glucose, adult	0.06–0.11 mM (51)	0.05–0.5 mM (148)

1.2. Detection of Human Skin

Clinically useful information such as skin temperature and physiological, electrophysiological, and biochemical cues can easily be obtained from the skin in a noninvasive manner. For instance, general physical activity, related body temperature, and cardiovascular activity elicit physiological responses from the skin. Electrophysiological responses are generated by the electrical activities of the brain, heart, and muscle. Sweat from the skin is a readily obtainable secretion that offers considerable information including pH and chemical composition (e.g., metallic ions, minerals, glucose, lactose, lactic acid, urea, volatile organic compounds), which can aid in accurate diagnosis of various health conditions (19). Analyzing tear film along with sweat can offer useful biochemical information. **Table 1** lists the physiological parameters of sweat and tear film. In adults, daily production of sweat and tear film can reach 10–14 L/day and 150–300 mL/day, respectively. The concentration of sodium ions in sweat (10–90 mM) is lower than that in tears (120–165 mM). Tear film contains relatively rich proteins that share similar constituents with blood (20). **Table 2** summarizes measurable cues from human skin, and their corresponding sensing modalities and obtainable biological information, which can be obtained by exploiting a range of skin-mountable devices.

2. SKIN-MOUNTABLE BIOSENSORS

Many skin-mountable devices provide multimodal sensing capabilities to detect not only strain, pressure, thermal, and electrophysiological signals from the skin but also biomarkers from sweat (21). This section reviews various types of sensing modalities and the working principles and device platforms of skin-mountable biosensors, along with their clinical implementations. Section 2.1 describes the various sensing modalities and related working principles of skin-mountable physical sensors, with a focus on materials, design layouts, and device platforms. Section 2.2 discusses skin-mountable electrophysiological sensors, with an emphasis on current challenges and opportunities in terms of practical implementation. Section 2.3 describes skin-mountable sensors tailored for detecting and analyzing sweat by exploiting a range of electrochemical sensing elements.

2.1. Skin-Mountable Physical Sensors

Monitoring physical skin responses such as strain and pressure can provide valuable biological information regarding health conditions (22–24). For example, skin-mountable sensors can be used for continuous collection of cardiogram data or monitoring of blood pressure during surgery (25). **Figure 2*a*** illustrates four different sensing methodologies, each of which relies on a piezoresistive, capacitive, piezoelectric, or iontronic mechanism. Piezoresistive and capacitive sensors capture changes in resistance and capacitance caused by external forces that cause geometric deformation (26, 27). Capacitive sensors are highly sensitive, but parasitic noise originating within the body and in the environment limits their performance (9). Piezoelectric sensors utilize polarization of

Table 2 Skin-related measurable cues and their corresponding sensing modalities and bioinformation

Measurable cues from human skin		Sensing modalities	Bioinformation	Physiological value range
Pressure/strain	Heart/respiration pulse Motion posture Cardiovascular motion	Piezoresistive sensing Capacitive sensing Piezoelectric sensing Iontronic sensing	Electrocardiogram Electroencephalogram Electromyogram Mechanomyogram Galvanic skin response Epilepsy Heart-rate monitoring	Electrocardiogram signal range, ~1 mV Electroencephalogram signal range, 10–100 μV Electromyogram signal range, ~5 mV Heartbeat for healthy resting adult, 60–100 beats (defined by the American Heart Association)
Temperature	Local body temperature	Resistometric sensing Field-effect transistor	An abnormal rise in body temperature due to fever General diseases or physical disturbances	Normal body (core) temperature range, 36.5–37.5°C Skin (mean) temperature range, 31.5–35.3°C
Sweat	Electrolytes (metal ions) Glucose Lactate Protein pH Skin humidity	Potentiometric sensing Amperometric sensing Voltammetric sensing Resistometric sensing Colormetric sensing	Moisture monitoring for dehydration Glucose monitoring for diabetes Levels of sweat metabolites and electrolytes for reflecting personalized health status	Normal blood Na^+ level, 135–145 mmol/L Normal blood K^+ level, 3.5–5.0 mmol/L Normal blood Cl^- level, 98–108 mmol/L Normal blood glucose level, 4.4– 6.1 mmol/L Normal blood lactate level, 1.4–2.3 mmol/L Normal sweat pH range, 7.35–7.45 Normal sweat conductivity range, 2,080–14,380 μΩ/cm

the embedded active material upon mechanical strain, leading to changes in the surface potential (26). Iontronic sensors utilize the electrical double layer of a supercapacitor platform in which the embedded ion gel interacts with electrodes to form double layers of charges on the surface. The capacitance can change as a result of external forces that squeeze the ion gel between the electrodes (28). Such iontronic methods are better suited for physical sensors due to their high initial capacitance, as they are less affected by external influences (29), but the difficulty of manufacturing them on a large scale and the toxicity of the ion gel impede their practical biomedical applications (9). **Table 3** summarizes the active materials used for several skin-mountable physical sensors and lists their corresponding sensitivities and detection limits.

Skin-mountable physical sensors can be utilized to detect skin lesions, control prosthetics, and analyze sleep disorder patterns. For instance, a study by Dagdeviren et al. (25) utilizes an array of piezoelectric materials, such as lead zirconate titanate (PZT) nanoribbons, into a flexible platform (**Figure 2*b***) in order to measure the viscoelasticity of human skin under static and dynamic conditions in a spatially controlled manner. The active conformal modulus sensor is constructed from a flexible network array of mechanical sensors and actuators, while the metal traces are designed in a serpentine format to efficiently accommodate mechanical strains under stretching. Such thin, flexible structures provide sufficient adhesion to skin through the van der Waals force alone. This

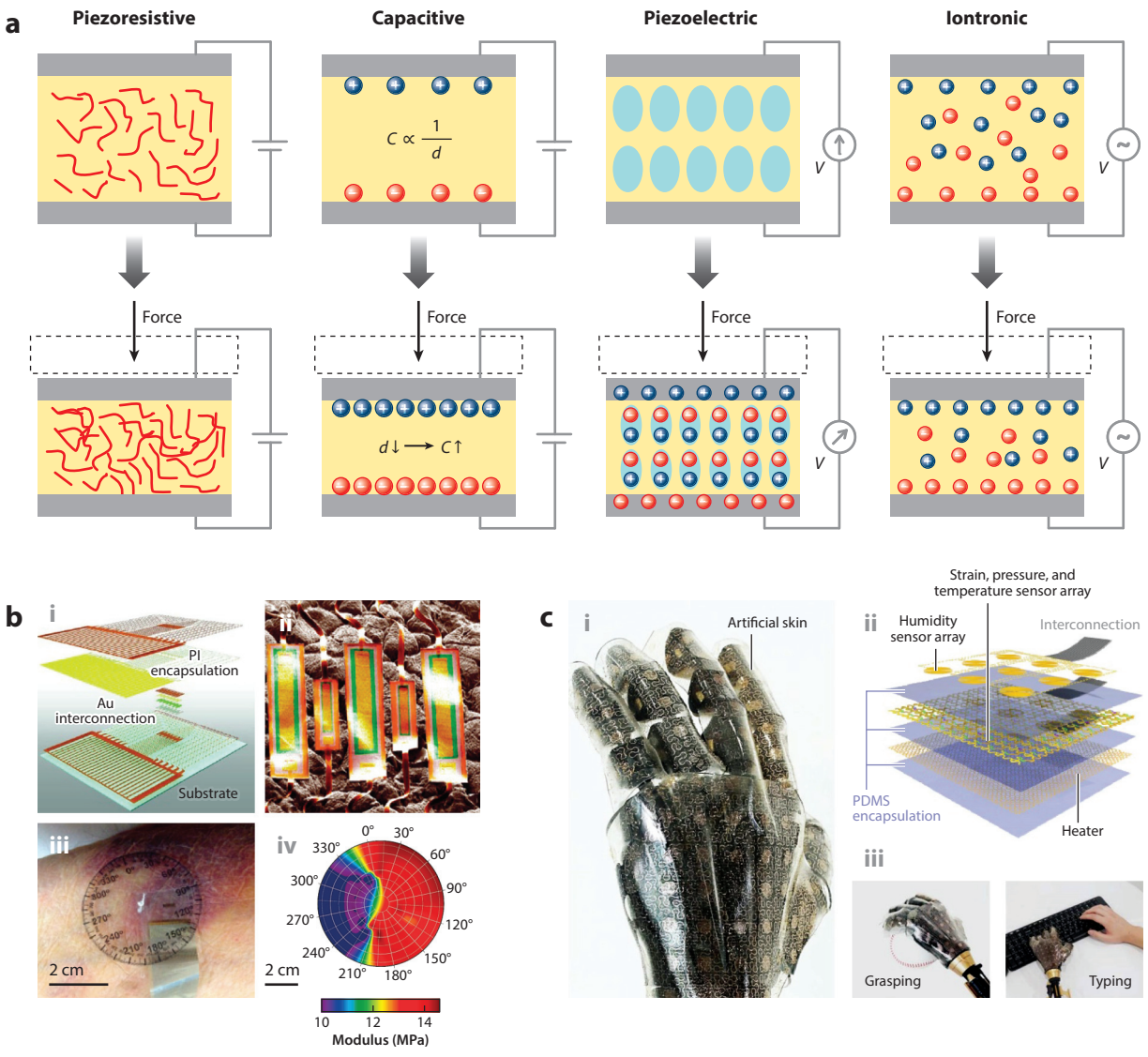

Figure 2

(*a*) Different types of mechanical sensing methods. (*b*) (*i*) Illustration of soft piezoelectric CMS constructed from flexible networks of mechanical sensors and actuators based on lead zirconate titanate nanoribbons. (*ii*) Colorization-processed scanning electron microscope image showing a CMS unit consisting of a sensor and actuator on artificial skin. (*iii*) Optical image showing the device mounted on the forearm. (*iv*) Mapping data (*clockwise from top right*) from the assessment. (*c*) (*i*) Optical image illustrating smart artificial e-skin with stretchable silicon nanoribbon electronics laminated onto a prosthetic hand. (*ii*) Schematic illustration of the device architecture of the smart e-skin. (*iii*) Optical images of the e-skin mounted on a prosthetic hand (*left*) grasping a baseball and (*right*) typing on a keyboard. Abbreviations: *C*, capacitance; CMS, compliant modulus sensor; *d*, distance; PDMS, polydimethylsiloxane; *V*, voltage. Panel *b* adapted with permission from Reference 25. Panel *c* adapted with permission from Reference 21.

Table 3 Various physical sensing modalities including tactile, pressure, and strain and their figures of merit

Mechanism	Sensing modality	Sensing element	Sensitivity	Unit	Detection limit	Unit	Reference
Piezoresistive	Tactile	Silicon nanoribbon	0.000315∼0.0041	kPa^{-1}	87	kPa	21
		Carbon nanotube	0.004	GF	50	kPa	111
		GO nanosuspension	0.0338	kPa^{-1}	7	mN	118
	Pressure	PEDOT:PSS	4.88∼10.3	kPa^{-1}	0.37∼5.9	kPa	112
		Galinstan	NA	NA	2.5	kPa	119
		Gold nanowire	>1.14	kPa^{-1}	13	Pa	113
	Strain	Carbon nanotube	0.06∼0.82	GF	NA	NA	114
		Platinum nanofiber	0.75∼11.45	GF	5	Pa	115
		Silver nanowire	2∼14	GF	NA	NA	116
		Graphene	10∼35	GF	NA	NA	117
		eGaLn	0.97∼3.57	GF	5%	Strain	120
Capacitive	Tactile	Carbon nanotube	0.034∼0.05	kPa^{-1}	0.4	Pa	121
		Gold	0.001∼0.01	kPa^{-1}	5∼405	kPa	122
	Pressure	Silver nanowire	0.88∼5.54	kPa^{-1}	8	Pa	123
		ITO	(8.4×10^{-5})∼0.45	kPa^{-1}	1∼1,800	kPa	124
	Strain	Carbon nanotube	1	GF	NA	NA	125
Piezoelectric	Strain	ZnO–paper	21.12	GF	NA	NA	126
	Pressure	PZT	0.005	Pa	10	Pa	127
		PVDF	0.1	Pa	12	Pa	128
Iontronic	Tactile	1-ethyl-3-methylimidazolium tricyanomethanide	0.43	nF/kPa	33	Pa	129
	Pressure	1-ethyl-3-methylimidazolium tricyanomethanide	29.8	nF/kPa	100	mN	130

Abbreviations: GF, gauge factor; GO, graphene oxide; ITO, indium tin oxide; NA, not applicable; PEDOT:PSS, poly(3,4-ethylenedioxythiophene) polystyrene sulfonate; PVDF, polyvinylidene fluoride; PZT, lead zirconate titanate.

device can be directly placed on basal cell carcinoma lesions to provide quantitatively measured spatial and directional mapping data on skin viscoelasticity.

Figure 2*c* shows another example of a skin-mountable physical sensor that includes an array of single-crystalline silicon nanoribbons that serve as the active piezoresistive element (21). The serpentine-patterned design enables the entire structure to withstand great strain, allowing integration with a prosthetic hand to provide the ability to sense temperature, strain, and pressure from the environment. The multifunctional sensing capabilities of this stretchable sensor can be useful in various everyday motions of the prosthetic hand, such as grasping an object or typing on a keyboard.

2.2. Skin-Mountable Electrophysiological Sensors

Electrophysiological recording is a crucial neurological methodology for diagnosis of many diseases, including epilepsy, dementia, dysphasia, and cardiac infection (30–36). Electrophysiological measurements may be performed using electrocardiography (ECG), electromyography (EMG),

or electroencephalography (EEG), depending on whether the electrical signal originates from the heart, muscles, or brain, respectively (13). Organ activity produces measurable time-dependent electrical surface potentials, allowing a pair of electrodes to capture electrophysiological signals from the skin (37).

Figure 3*a* illustrates three different contact methods, namely wet, dry, and capacitive contact, along with the corresponding equivalent electrical circuits (37, 38). Typically, electrophysiological

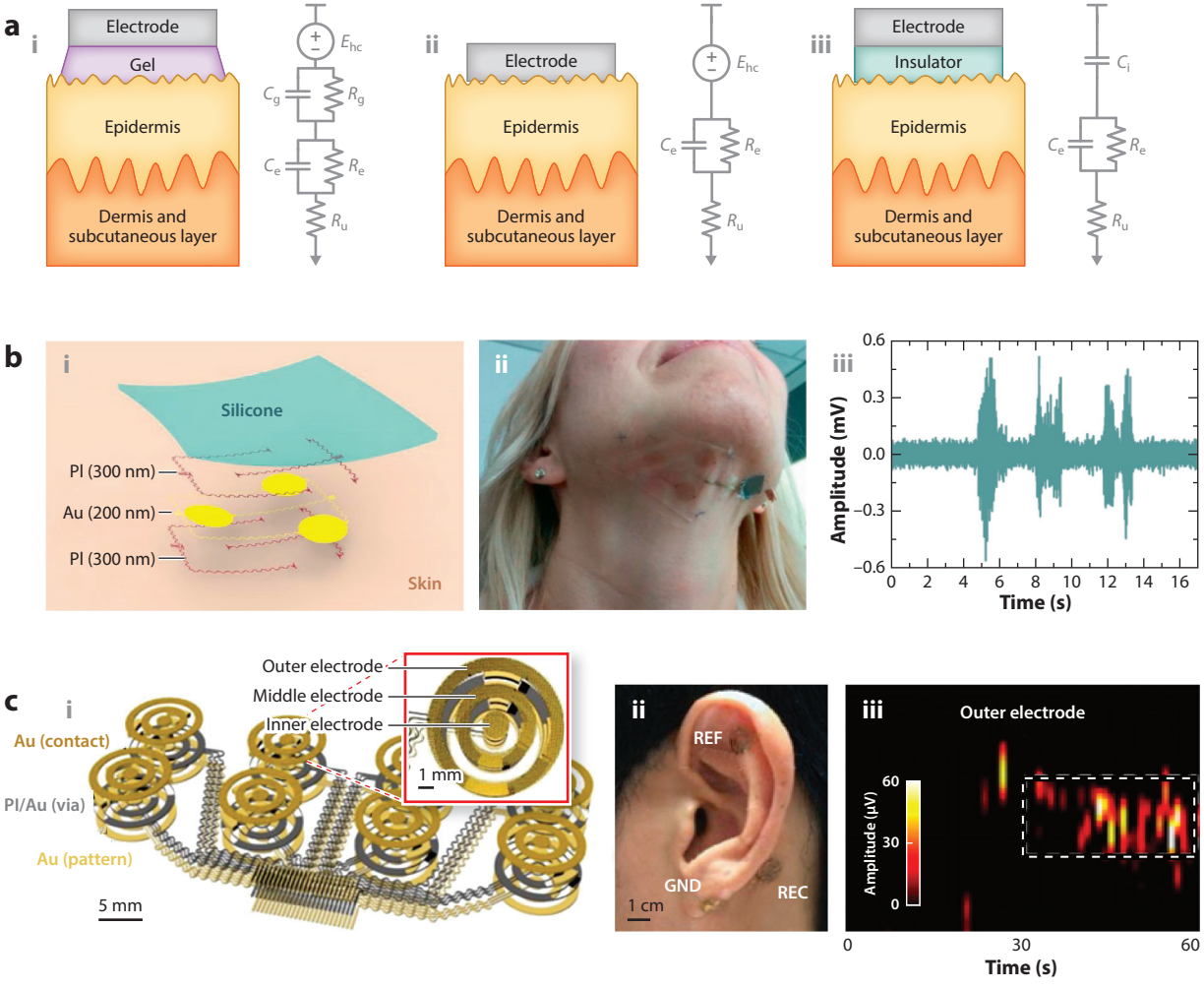

Figure 3

(*a*) Different types of electrical connection between a device and the skin and their equivalent electrical schematic diagrams. (*b*) (*i*) Schematic configuration of an sEMG electrode. (*ii*) Epidermal sEMG patch worn on a person's chin. (*iii*) Sample signal collected during three saliva swallows by the epidermal sEMG patch with an integrated reference. (*c*) (*i*) Integrated set of electrodes on the auricle and mastoid mounted on skin. (*Inset*) Close-up optical image of the device. (*ii*) Epidermal electronics with a tripolar concentric ring composed of three electrodes (REC, GND, and REF) and an interconnect. (*iii*) Spectrograms of EEG alpha rhythms recorded by the device. The dashed box highlights the increase in power of EEG alpha rhythms, with a frequency of around ~10 Hz, after the subject closes their eyes. Abbreviations: C_e/R_e, equivalent epidermal capacitance/resistance; C_g/R_g, gel capacitance/resistance; C_i, insulation capacitance; EEG, electroencephalography; E_{hc}, half-cell potential; R_u, resistance underlying dermis and hypodermis; sEMG, surface electromyography. Panel *b* adapted with permission from Reference 41. Panel *c* adapted with permission from Reference 42.

signals on the skin have an electrical potential level of <2 mV. For reliable measurements, the input impedance of the differential amplifiers should be at least 10 times higher than the electrode impedance, which is typically between 5 and 50 kΩ. Wet-contact electrodes contain silver/silver chloride (Ag/AgCl) as well as an electrolyte gel that serves as an ion-conductive medium. These electrodes are the most frequently used due to their affordable cost and reliable electrical performance, but they are not suitable for long-term use because the signal degrades when the electrolyte gel dries out (39). By contrast, dry-contact electrodes can offer a longer lifetime and may eliminate possible allergic effects associated with the electrolyte gel or Ag/AgCl electrodes. Achieving seamless contact between dry-contact electrodes and the skin is crucial, because any air gap, mainly due to hair or roughness of the skin, results in a degraded signal. For capacitive-contact electrodes, there is no direct electrical contact with the skin due to the presence of a dielectric layer. This is beneficial in terms of improved electrical safety and reduced potential skin irritation, but devices with capacitive contacts are sensitive to external electric fields from moving charges in the environment due to the high input impedance. Often, a grounded shield is required for such devices in order to reduce charge interference from the environment (38, 40).

Figure 3*b* summarizes research by Constantinescu et al. (41) that involves a thin, flexible skin-mountable EMG sensor patch for dry-contact-based measurement of muscle activity during swallowing in a patient with dysphagia (i.e., difficulty swallowing). The device is composed of a thin-film layer (200 nm) of gold encapsulated by a polyimide layer (300 nm) on both sides, all mounted on a soft silicone substrate. The thin, flexible property of the sensor allows highly conformal, seamless integration onto the human skin, thereby improving the quality of signal acquisition. This study demonstrates that such skin-mountable EMG sensor patches can be robust against motion artifacts compared with conventional systems (7179-0020-Demo/XP; Pentax Canada, Inc., Mississauga, Canada).

Figure 3*c* presents a similar type of skin-mountable EEG sensor patch, developed by Norton et al. (42), used to measure brain activity. The use of a tripolar concentric ring design and capacitive-contact electrodes provides sufficient spatial resolution and mechanical robustness under multiple cleaning steps with soap, water, or isopropyl alcohol antiseptic. The spectrogram of the EEG alpha rhythm measured by use of the ring-shaped electrodes (**Figure 3*c***) shows the increased power (~10 Hz) of the EEG signal after the subject's eyes were closed (30–60 s).

2.3. Skin-Mountable Electrochemical Sensors for Sweat

Human sweat contains ions, such as Na^+, K^+, Ca^+, and Cl^-, as well as small molecules, such as lactate, glucose, urea, sugar, protein, peptides, and ammonia, providing plentiful important biological information that can potentially be used for diagnosis (8, 43–47). For instance, detection of Cl^- or lactate in sweat can indicate cystic fibrosis in infants (48) or tissue hypoxia (49), respectively. In addition, detection of uric acid and creatinine concentration may be useful in identifying kidney-related diseases. Likewise, continuous monitoring of Na^+ and Cl^- in sweat or the local sweating rate during an exercise can provide fundamental indicators of homeostatic malfunction (49) and hyperhidrosis, which can cause autonomic dysfunction and seizures (49), respectively.

The recent development of skin-mountable electrochemical sensors enables noninvasive, continuous monitoring of multiple biomarkers from human sweat and, therefore, can improve outcomes in diagnostic applications (50–52). **Figure 4*a*** highlights several important aspects of the use of electrochemical sensors for sweat, namely the sensing mechanisms, platforms, and performance (also see **Table 4**).

Widely used materials for electrochemical sensors for sweat include carbon-based materials (53), functionalized conducting polymers with enzymatic assays (54), metallic nanoparticles (55),

multidyes (56), and two-dimensionally or multidimensionally structured materials (57). For instance, Zhong and colleagues (58) utilized a flexible form of cellulose nanofibrous membrane decorated with gold nanoparticles for accurate detection of salt and moisture in sweat. This study used molecularly imprinted polymers (MIPs) to detect cortisol in sweat by exploiting poly(3,4-ethylene dioxythiophene) polystyrene sulfonate (PEDOT:PSS) transistors (59). Methacrylic acid

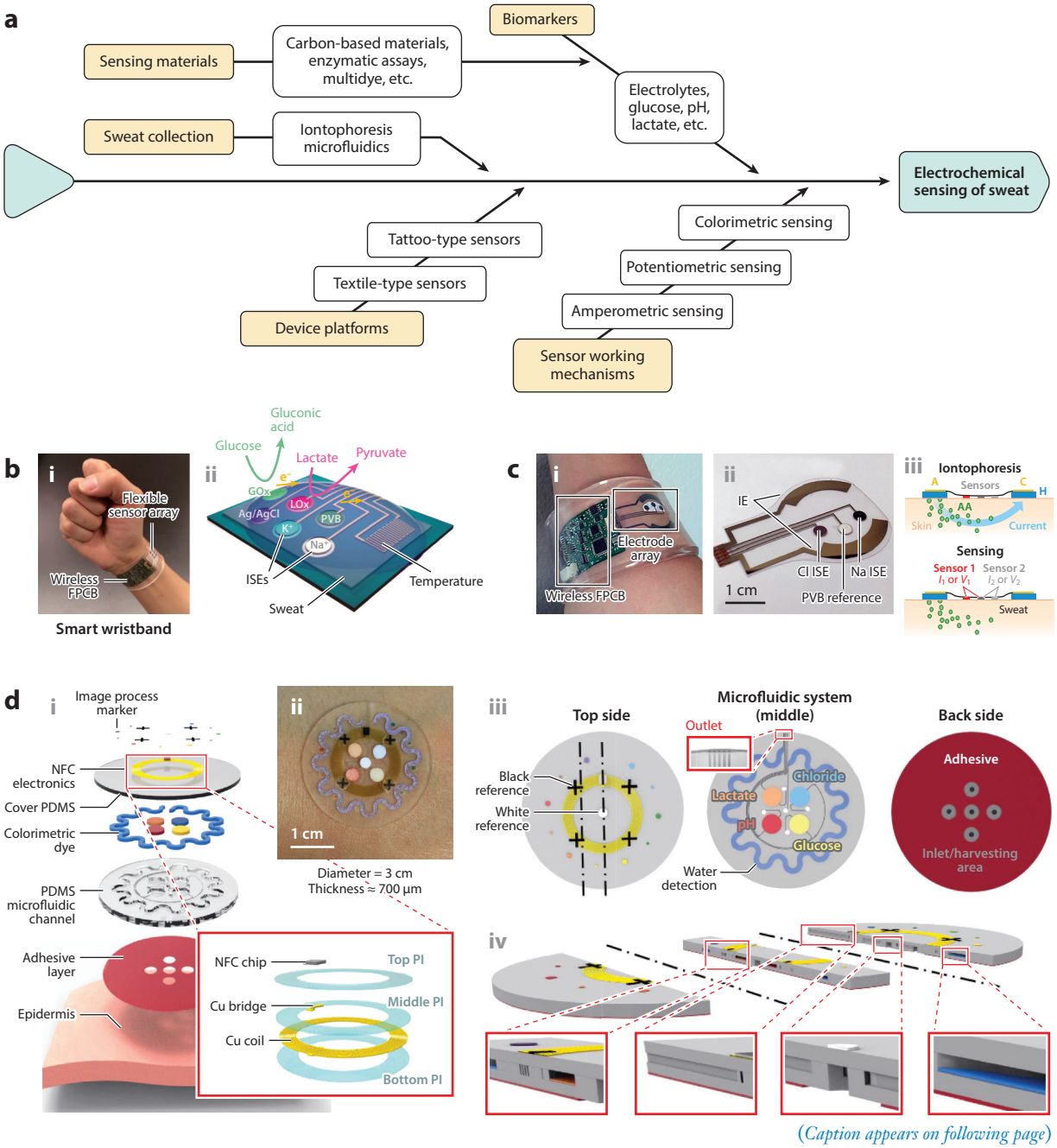

(*Caption appears on following page*)

Figure 4 (*Figure appears on preceding page*)

(*a*) Fishbone diagram of electrochemical sensing of sweat, showing important parameters. (*b*) (*i*) Photograph of a wearable, flexible, integrated sensing array on a subject's wrist, integrating the multiplexed sweat sensor array and the wireless FPCB. (*ii*) Schematic of the sensor array (including glucose, lactate, sodium, potassium, and temperature sensors) for multiplexed perspiration analysis. (*c*) (*i*) Image of autonomous sweat extraction and (*ii*) corresponding sensing platform. (*iii*) Schematic illustrations of the iontophoresis and sensing modes. (*d*) (*i*) Schematic illustration of an epidermal, microfluidic sweat-monitoring device. (*Inset*) Enlarged image of the integrated NFC system. (*ii*) Optical image of a fabricated device mounted on a patient's forearm. (*iii*) Illustration of the top, middle, and back of the device. (*iv*) Cross-sectional diagrams of the microfluidics. Abbreviations: A, anode; AA, agonist agent; C, cathode; FPCB, flexible printed circuit board; GOx, glucose oxidase; H, hydrogel; IE, iontophoresis electrodes; I_1 and I_2, current measured from sensors 1 and 2; ISE, ion-selective electrode; LOx, lactate oxidase; NFC, near-field communication; PDMS, polydimethylsiloxane; PVB, polyvinyl butyral; V_1 and V_2, voltage measured from sensor 1 and 2. Panel *b* adapted with permission from Reference 47. Panel *c* adapted with permission from Reference 71. Panel *d* adapted with permission from Reference 60.

as a monomer, mixed with cortisol as a template, is polymerized; then the cortisol in the polymer is removed through a mixture of acetic acid and methanol in order to form MIPs. The PEDOT:PSS transistors with MIPs showed improved sensitivity (2.68 μA/dec per order of magnitude change in concentration of cortisol).

Electrochemical sensors employ several different sensing mechanisms. For instance, amperometry-based sensing compares the difference in electrical current in conducting materials between an anode and a cathode (49). Potentiometry-based sensing measures the potential of a solution between reference and indicator electrodes, where the indicator electrode is modified with ion-selective materials. Once targeted ions are bound to the surface of an indicator electrode, the potential difference between the electrodes can be correlated to the targeted ion in sweat. Colorimetry-based sensing in clinical practice is to assess a variety of chemical information, such as the pH of human secretions and glucose. Portable devices such as smartphones can be used to detect subtle changes in color arising from the detection of an analyte (60–63).

Wearable platforms also employ different types of electrochemical sensors. For instance, Gao et al. (47) developed wristband- and headband-type multiplexed sensors that enable both physiological and electrochemical measurements (**Figure 4*b***). This sensor is designed to detect K^+, Na^+, glucose, lactose, and sweat temperature; transduce the biological signals to electrical signals; and transfer the signals to the wearer in a wirelessly controlled fashion. Amperometric electrochemical sensors covered with a permeable linear polysaccharide chitosan film detect glucose and lactate in sweat through enzymatic reactions with glucose and lactate oxidase.

Other platforms for skin-mountable electrochemical sensors include textile- and tattoo-type sensors. In textile-based sweat sensors, electrically conductive fabric materials can be prepared by inkjet printing (64), the stamp transfer method (65), dip coating, and screen printing of an Ag/AgCl paste on commercially available fabrics (66, 67). Coating of PEDOT:PSS (68) on a fabric substrate, direct wet-spinning of a mixture of matrix polymers, and the use of conductive materials such as single-walled carbon nanotubes (69) and PEDOT:PSS are typical approaches to the preparation of conductive textiles for nonmetallic sweat sensors. Bandodkar et al. (70) developed an all-printed temporary tattoo–type glucose sensor for noninvasive glycemic monitoring. This sensor uses a reverse-iontophoresis mechanism to efficiently extract glucose from an interstitial fluid. The device is functionalized with glucose oxidase enzyme incorporated with chitosan biopolymer on the amperometric biosensor. This study demonstrates that the sensor responds to the addition of 10 μM glucose and transduces the signals linearly in a consistent manner (sensitivity, 23 nA/μM; limit of detection, 3 μM).

For accurate electrochemical sensing, it is necessary to collect enough sweat to ensure a sufficient concentration of biomarkers. **Figure 4*c*** shows an approach that exploits iontophoresis to painlessly extract sweat from a specific area of the skin; an agonist agent can be introduced

Table 4 Electrochemical sweat sensing mechanisms

Sensing mechanism	Sensing platform	Recognition element	Analytes	Detection range	Unit	Sensitivity	Unit	Reference
Amperometry	Gas-permeable membrane	Platinum	Dissolved oxygen	0–8.0	mg/L	NA	NA	131
	Cotton (underwear)	Bare carbon	NADH, H_2O_2	0–100 for NADH, 0–25,000 for H_2O_2	μM	NA	NA	132
	Electronic patch	rGO and chitosan–glucose oxidase composites	Glucose	0–2.4	mM	48	$\mu A/(mM \cdot cm^2)$	133
	Microfluidics	Lactate oxidase	Lactate	4–20	mM	29.6	μM/μA	134
Potentiometry	Polyimide/Lycra blend	Sodium ionophore	Sodium	60	mM	NA	NA	135
	Polyester	Ag/AgCl	Chloride	10–100	mM	NA	NA	136
	Temporary tattoo	Polyaniline	pH	3–7	pH	50.1	mV/pH	137
		Ammonium ionophore	Ammonium	10^{-4}–0.1	M	NA	NA	138
		Sodium ionophore	Sodium	NA	NA	60.41	$mV/\log_{10}[Na^+]$	139
Conductometry	Parylene skin patch	Lactate oxidase	Lactate	0.3–1.3	mM	NA	NA	140
Voltammetry	Elastomeric stamps	Bare carbon	Uric acid	2–10	mM	0.971	μA/mM	65
Colorimetry	Microfluidics	Glucose oxidase	Glucose	0–25	mM	NA	NA	60
		D-Lactase assay kit	Lactate	0–100	mM	NA	NA	60
		Chloride assay kit titrated with $Hg(SCN)_2$	Chloride	0–625	mM	NA	NA	60
		Creatininase, 4-aminophenazone	Creatinine	0–1,000	μM	NA	NA	60

Abbreviations: NA, not applicable; rGO, reduced graphene oxide.

between the skin and the iontophoretic device for the patient's comfort (71). The integration of iontophoresis and various sensing elements (Na^+, Cl^-, and glucose) enables the programmable collection of sweat and real-time analysis for use in quantifying Na^+, Cl^-, and glucose.

A thin elastomeric microfluidic platform that can be flexibly attached to the human skin was recently developed to efficiently collect and store sweat in a microreservoir during physical activity (50). The difference in osmolality between blood plasma and sweat can generate pressure in sweat glands, inducing a flow of sweat from the embedded microfluidic channels to the microreservoir. Capillary burst valves in the microfluidic channels are used to precisely control the flow of sweat, enabling chronosampling. When the sweat encounters two separate capillary burst valves with different burst pressures, it proceeds first via the lower-burst-pressure valve at a designated pressure. Likewise, the direction of sweat flow can be controlled by two capillary burst valves with different burst pressures at the intersection of the microfluidic channels.

Figure 4*d* presents an example of a microfluidics-based sweat collection platform that consists of multilayered stacks of subsystems: (*a*) a skin-compatible adhesive layer with micromachined openings that define the areas of sweat collection, (*b*) a sealed collection of soft microfluidic channels and reservoirs filled with color-responsive materials for quantitative analysis of sweat volume and chemistry, and (*c*) a magnetic loop antenna and corresponding near-field communication electronics for wireless data communication to and from external devices (60). The colorimetric analysis of sweat in this study provides the concentration of chloride, glucose, lactate, and pH in a highly convenient manner simply by using the skin-mountable patch.

3. SKIN-MOUNTABLE THERAPEUTICS AND DRUG DELIVERY SYSTEMS

The growing demand for patient-friendly therapies has led to the development of skin-mountable therapeutics and drug delivery systems that offer advantages over conventional approaches in terms of efficacy and ease of use (72–74). This section discusses several applications of skin-mountable therapeutics and drug delivery systems in emerging health care and biomedical applications. Section 3.1 reviews therapeutic devices that utilize electrical stimulations to regulate cellular treatments and control drug dosages for the human body. This section describes the most commonly used therapeutics and neuroprosthetic applications of neuromuscular electrical stimulation regarding rehabilitation of upper and lower extremities, as well as the recent development of a skin-mountable electronic heater platform. Section 3.2 reviews therapeutic methodologies that exploit transdermal drug delivery systems.

3.1. Skin-Mountable Therapeutic Stimulation Methods

Functional electrical stimulation (FES) is a common method in which a safe level of electrical current is applied through the skin to stimulate muscle activity (75). This technique is particularly useful for patients whose motor functions are affected by central nervous system lesions caused by spinal cord injury, stroke, or other neurological disorders (76–78). FES requires two pairs of conducting electrodes to deliver electrical current across them. Similarly, in physiotherapy thermal stimulation is widely used to mitigate joint injuries and aid rehabilitation by increasing blood flow via expansion of the vascular system (79–81). Traditional approaches involve the application of preheated heat packs onto the skin of the affected area, whereas more advanced methodologies using electronically controlled heating packs allow controlled point-of-care thermal stimulation to enhance the therapeutic effects.

Figure 5*a* shows an example of a dry-contact-type FES that includes an array of 24 carbon-loaded silicone rubber electrodes on a flexible and breathable polyester–cotton fabric substrate suitable for long-term use (82). Pointing, pinching, and open-hand gestures are induced by selectively stimulating the muscle fibers of the forearm via the FES sensor array. Such devices can serve as assistive electrical stimulators to assist patients with central nervous system lesions who have difficulty with everyday movement.

Figure 5*b* displays a device developed by Xu et al. (83) that includes an integrated electronic system comprising both FES and an EMG sensor, wherein an array of electrodes is fabricated on a

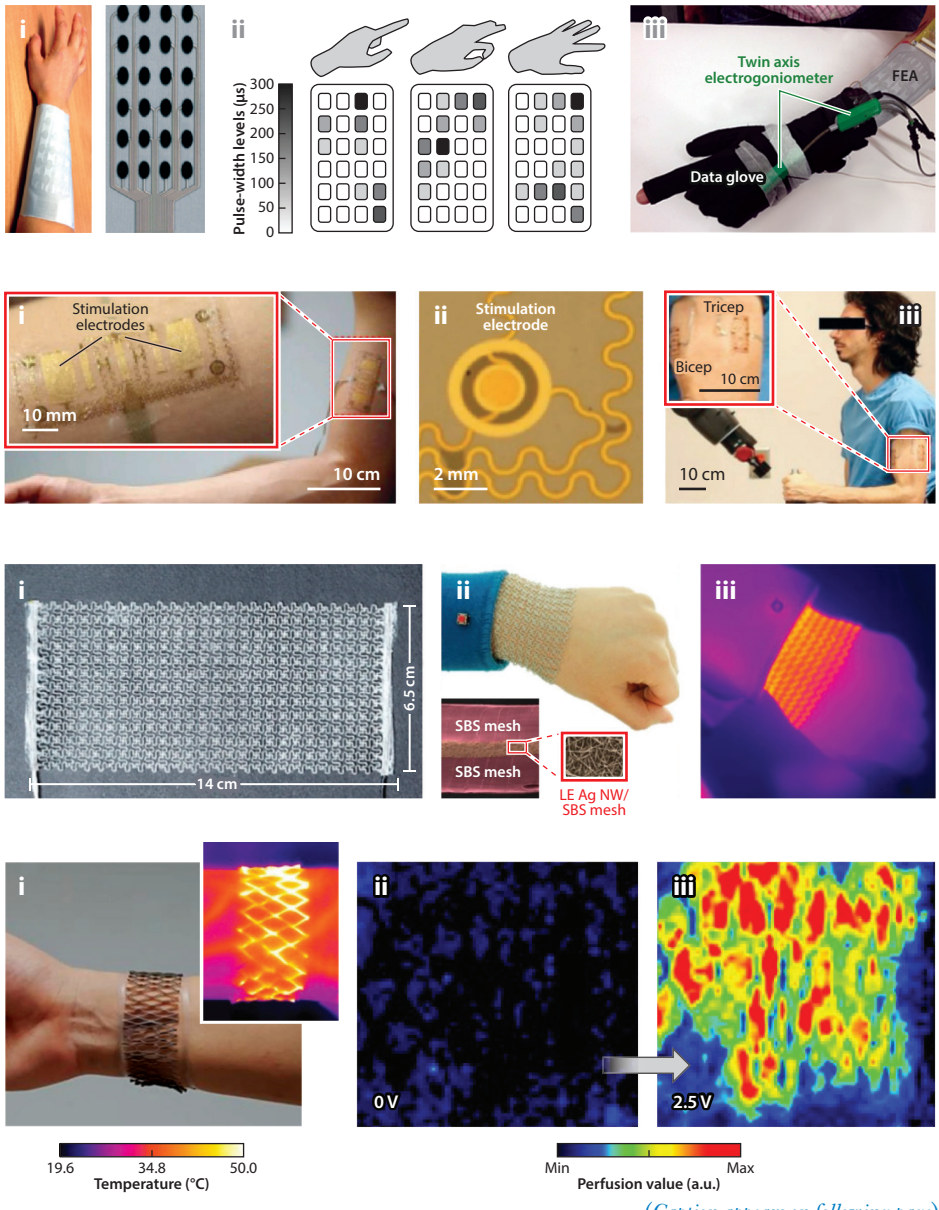

(*Caption appears on following page*)

Figure 5 (*Figure appears on preceding page*)

(*a*) (*i*) Optical image of fabric electrode and flexible PCB array for electrical stimulation of the forearm. (*ii*) Diagram corresponding to the electrode array, indicating the pulse-width levels of stimulation pattern for pointing, pinching, and open-hand gestures. (*iii*) Electrical stimulation and measurement of each hand gesture. (*b*) (*i*) Epidermal device with large-area electrodes for electrical muscle stimulation mounted on the bicep. (*ii*) Microscope image of the electrical stimulation electrode. (*iii*) Optical image of a volunteer controlling a prosthetic robot with stimulation feedback. (*c*) (*i*) Image of a large-area stretchable heater using an LE Ag NW nanocomposite. (*ii*) Photograph and (*iii*) corresponding IR thermal image of the large-area heater worn on the wrist with activation of thermotherapy. (*d*) (*i*) Image of a skin-mountable heater made from a stretchable kirigami conductor worn on the wrist. (*Inset*) Corresponding IR thermal image. (*ii*, *iii*) Blood-flow characterization of color Doppler images, showing blood perfusion on the human wrist; comparison is between heater off (*ii*) and on (*iii*). Abbreviations: Ag NW, silver nanowire; FEA, finite-element analysis; LE, ligand-exchanged; PCB, printed circuit board; SBS, styrene–butadiene–styrene. Panel *a* adapted with permission from Reference 82. Panel *b* adapted with permission from Reference 83. Panel *c* adapted with permission from Reference 79. Panel *d* adapted with permission from Reference 84.

thin layer (60 μm) of silicone elastomer. The EMG signal measured on the bicep is used to control a prosthetic hand, while a sensor located inside the grip aperture measures the force applied and provides proprioceptive feedback through the FES at a level proportional to the measured force. The feedback data are used to help the test subject precisely control the level of grasping force, and can therefore prevent the application of excessive force on the object being grasped.

Figure 5*c* presents an example of a skin-mountable articular thermotherapy device that consists of conducting silver nanowires and physically cross-linked styrene–butadiene–styrene (SBS) elastomer (79). The silver nanowires must be modified from hydrophilic to hydrophobic via ligand-exchange reaction, as hydrophilic nanowires do not disperse in the SBS solution. The resulting composite is connected to an electronic band that includes (*a*) a battery for wireless powering, (*b*) a microcontroller unit to control the heating process in a preprogrammed manner, and (*c*) an automatic shutdown unit to prevent potential skin damage due to low-temperature burns. The IR thermal image in the figure displays the uniformly distributed heat over the wrist of a test subject during conformal contact with the skin under various deformations.

Figure 5*d* presents a device developed by Jang et al. (84) that employs a highly stretchable heater using aluminum-doped conductive paper. The device is fabricated by immersing pristine paper sheets into an aluminum hydride solution that contains aluminum precursors, followed by coating with a catalyst solution (mixture with 5 vol% of titanium isopropoxide and 95 vol% of dibutyl ether). The aluminum-doped conductive paper is embedded inside a prepatterned elastomeric substrate with a kirigami-inspired layout, allowing the entire structure to be stretched up to ∼400% without generating any defects or causing degradation in performance. The fabrication process is simple, rapid, and scalable enough for high-volume manufacturing, and therefore could produce cost-effective skin-mountable heaters.

3.2. Skin-Mountable Drug Delivery Systems

Transdermal drug delivery through skin-mountable patches has gained traction due to its non-invasiveness and painless administration (2, 85, 86). The recent development of skin-mountable transdermal drug delivery systems allows controlled release of drug molecules through the skin at the desired dose; the releasing mechanism relies on external forces, microneedle injections, or an electronic trigger (87–92). Such systems can provide a precise route of delivery at the correct frequency and timing, which can improve patient adherence to complicated regimens and lessen anxiety associated with drug administration (93).

Figure 6*a* shows the evolution of skin-mountable drug delivery systems with respect to their components and drug-releasing mechanisms (2, 86). The first generation of devices was not

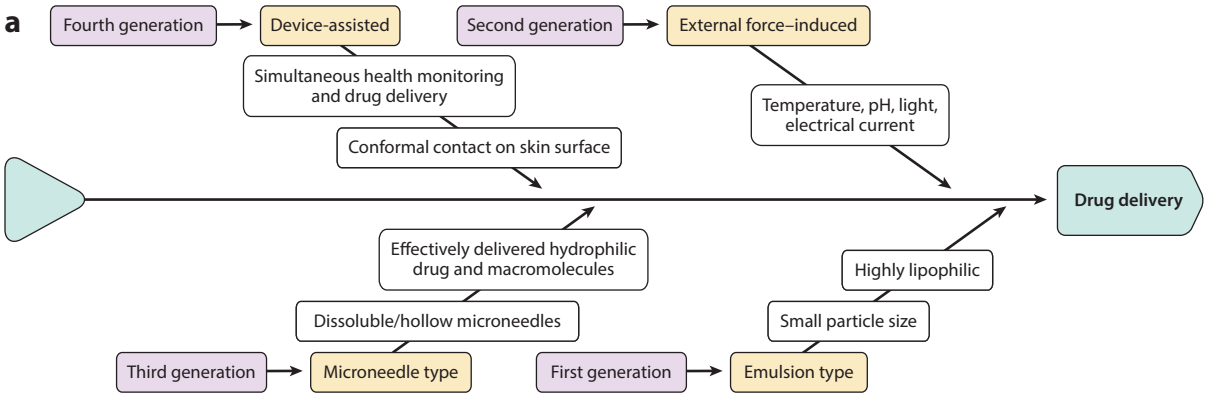

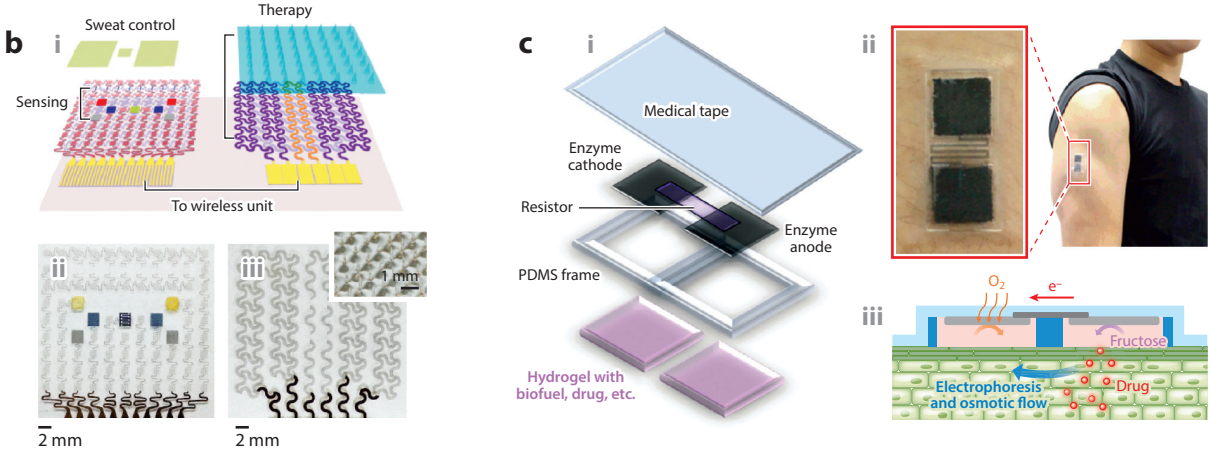

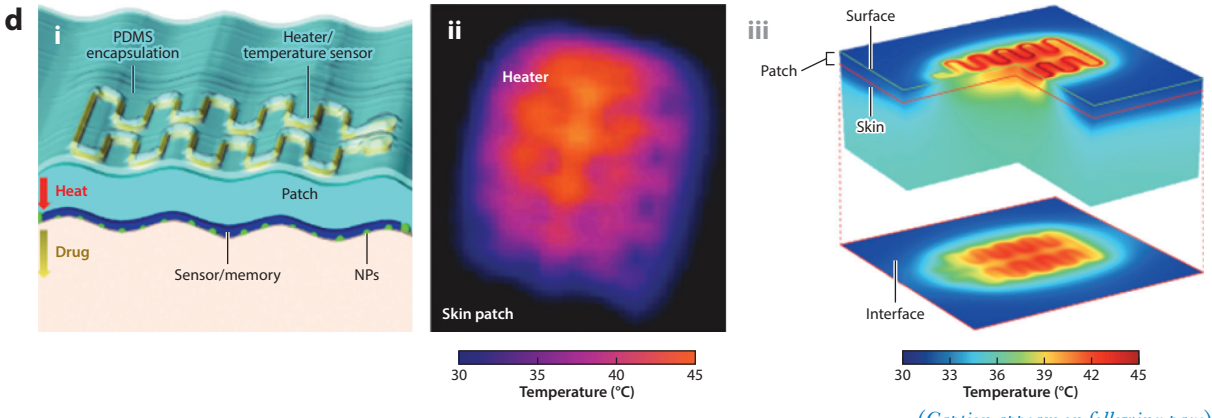

(Caption appears on following page)

Figure 6 (*Figure appears on preceding page*)

(*a*) Fishbone diagram of various drug delivery systems, with corresponding working principle types and key features. (*b*) (*i*) Schematic drawings of the diabetes patch, which is composed of sweat-control, sensing, and therapy components. (*ii*) Optical camera image of an electrochemical sensor array. (*iii*) Therapeutic array. (*Inset*) Magnified view of drug-loaded microneedles. (*c*) (*i*) Schematic of a transdermal iontophoresis patch comprising an assembly of enzyme-modified carbon fabrics. (*ii*) Photograph of the patch mounted on a human arm. (*iii*) Schematic of the iontophoresis-assisted drug delivery mechanism. (*d*) (*i*) Schematic illustration of controlled transdermal drug delivery from hydrocolloid and mesoporous-silica NPs by thermal actuation. (*ii*) Temperature distribution measurement of the heater on the skin patch using an IR camera. (*iii*) Finite-element model of the three-dimensional thermal profile of a heater on the patch and at the interface between the patch and the skin. Abbreviations: NP, nanoparticle; PDMS, polydimethylsiloxane. Panel *b* adapted with permission from Reference 94. Panel *c* adapted with permission from Reference 99. Panel *d* adapted with permission from Reference 100.

optimized for delivery of various kinds of drug molecules through the skin due to the molecules' high partition coefficients ($>10^4$), high molecular weight (>400 Da), and large particle size. Modification of drug formulations through the use of emulsions, nanocarriers, and chemical enhancers has improved the process of diffusion through the skin. In the second generation of devices, chemical enhancers or external energy sources were employed to increase the efficiency of the drug molecules' permeability through the stratum corneum of the skin without causing damage (2, 86). External stimuli such as heat and electrical stimulation from the external device can be used to increase the efficacy of drug administration. In the third generation, a skin-mountable patch embedded with minimally invasive microneedles was used to effectively transfer hydrophilic drugs and macromolecules into the inner layer of skin, such that damage to the epidermis was minimized. The most challenging issue arose from the difficulty of removing microneedles following drug delivery (2). A way to circumvent this problem involves the use of bioresorbable microneedles, but a challenge remains concerning how to fabricate bioresorbable microneedles without degradation while maintaining a high quantity of drug molecules during polymerization (95, 96). In the fourth generation of devices, controlled release of drug molecules occurs through an electronically manipulated triggering unit that typically contains miniaturized sensors (97, 98). There is great demand for autonomous sensors and transdermal drug delivery devices, but further improvements are needed.

Figure 6*b* shows an example of a skin-mountable drug delivery system that can monitor sweat from patients with diabetes and simultaneously provide feedback therapy such as drug delivery (94). The drug delivery system consists of a thermal heater controlled by the feedback of a graphene-based temperature sensor and a temperature-responsive drug-loaded microneedle array. Bioresorbable microneedles made of polyvinyl pyrrolidone can be incorporated into this patch platform; the microneedles are coated with a thermal phase-change material (tridecanoic acid) and can sequentially release the drug molecules in a programmed manner by generating heat to activate the phase change.

Figure 6*c* depicts another example of a skin-mountable drug delivery system that consists of (*a*) enzyme-modified carbon fabrics used as electrodes, (*b*) a PEDOT:PSS and polyurethane composite as a conducting polymer, (*c*) hydrogel films containing fructose as well as ascorbyl glucoside and rhodamine B as drug compounds, (*d*) a polydimethylsiloxane frame as a drug reservoir, and (*e*) oxygen-permeable medical tape as a substrate (99). This device is powered by enzymatic biofuel cells that generate an iontophoretic current through an enzyme-catalytic reaction involving the oxidation of fructose. When mounted on the skin, the patch generates a transdermal ionic current with osmotic flow from anode to cathode, thereby administering the drug through the skin.

Figure 6*d* shows a multifunctional skin-mountable device that contains units for data storage, diagnostics, and drug delivery, allowing simultaneous diagnosis and therapy (100). The embedded nonvolatile resistance memory devices provide the ability to regulate thermal actuators through

the programmable release of drug molecules. A compelling future application for sensing and data storage will be to employ in-sensor analytics that can recognize the characteristic pattern of diseases and then trigger the onset of drug administration in an on-demand manner. This device utilizes dye-loaded mesoporous silica nanoparticles (101, 102) as a drug-containing and drug delivery vehicle with low cytotoxicity and excellent chemical stability.

4. SOFT PACKAGING MATERIALS AND SCHEMES

Mechanically soft packaging of skin-mountable devices is crucial not only to protect the electronic components from humidity, temperature, and mechanical load but also to provide sufficient adhesion to the skin with high fidelity in order to accommodate mechanical strain induced by skin deformations. The conventional chip-scale packaging technique involves high-temperature soldering on a rigid inorganic substrate and complex array configurations (103), which limit the use of soft elastomeric substrates due to melting (104–106). The recent development of soft materials has enabled nearly imperceptible physical contact between a skin-mountable device and human skin by precisely modulating the material's mechanical properties so that they are similar to those of skin (13, 107, 108). For instance, Xu et al. (109) developed a core/shell packaging strategy by incorporating soft, viscous fluidics and elastomeric silicones in the core and shell layers, respectively. Their system (**Figure 7*a***) is composed of a microfluidic enclosure, a free-floating interconnect network, and integrated circuits (amps, radios, sensors); the chip-level components are electrically connected to the interconnect network using low-temperature solder. The metal traces can freely move, twist, and deform within the microfluidic space. The device can be directly laminated onto the skin to capture real-time data from skin temperature measurements, ECG, EMG, EEG, and electrooculography in a wireless-controlled manner. However, the use of fluidics in the core materials presents a potential risk of fluid leakage through excessive skin deformation.

Figure 7*b* shows another type of core/shell packaging strategy that includes an ultralow-modulus elastomer [Silbione; mechanical modulus (E) $\approx$ 5 kPa] and a thin layer of silicone (Ecoflex, $E \approx 60$ kPa) for the core and shell layers, respectively (110). The use of an ultralow-modulus elastomer instead of fluid can eliminate the possibility of fluid leakage. In this scheme, the outer shell layer provides the necessary roughness for handling and laminating of the device onto the skin; the embedded rigid chip-scale components, including accelerometers, temperature sensors, Bluetooth chip, and battery, are placed in the center and mechanically isolated from their surroundings. The device is capable of maintaining highly conformal, seamless contact with the skin in a manner that can minimize interfacial stress. This device demonstrates real-time wireless monitoring of skin temperature and three-axis body motion of a test subject during exercise.

5. CONCLUSION AND OUTLOOK

In this review, we have discussed strategies for the use of various skin-mountable devices in clinical diagnosis and therapy. Point-of-care wearable devices that can alleviate time and space constraints are emerging due to a shift in the health care paradigm toward home monitoring, disease management, and prevention. The recent development of mechanically soft materials and flexible electronics has enabled conformal, seamless contact between the devices and the skin, which is crucial for accurate measurements of physical, electrophysiological, electrochemical, and biological signals as well as for transdermal delivery of therapeutic stimulation and drugs. Strategies to integrate multimodal sensors and stimulators within a single device are being continuously improved, with the goal of autonomous operation. Established skin-mountable platforms can be integrated with

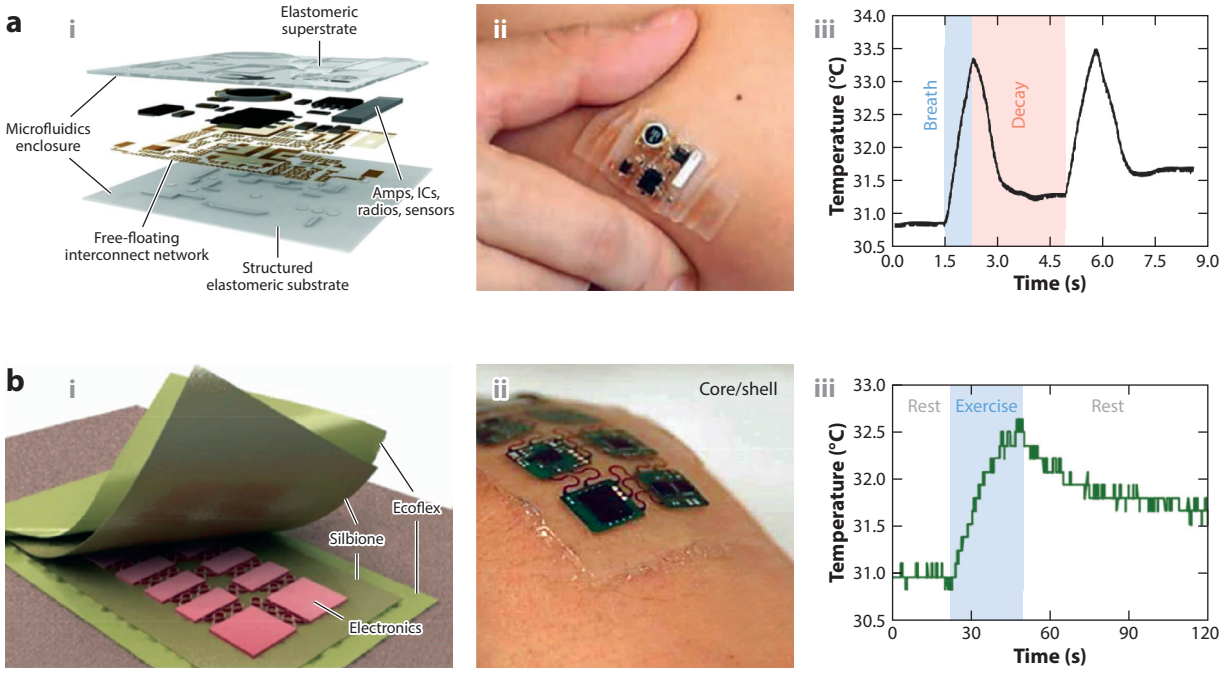

Figure 7

(*a*) (*i*) Schematic illustration of component layers of the system in soft microfluidic assemblies. (*ii*) Optical images of the device mounted on the forearm. (*iii*) Temperature measurement of the device in real time placed under breaths of warm air. (*b*) (*i*) Schematic illustration of an Ecoflex (shell)/Silbione (core) packaging system with a peel-away view at one of the corners. (*ii*) Optical images of a core/shell structure, with commercially available wireless electronics laminated onto the wrist. (*iii*) Real-time monitoring of a temperature change during exercise and during rest. Abbreviation: IC, integrated circuit. Panel *a* adapted with permission from Reference 109. Panel *b* adapted with permission from Reference 110.

an array of flexible microfluidics and lab-on-a-chip sensors, enabling continuous monitoring and analysis of sweat; however, currently used biological receptors are limited by low repeatability for practical applications. Further improvements in the stability, selectivity, cohesion, and production costs of these sensors are required. Various biological data collected from patients will be crucial in implementing precise and preventive care, wherein patient data privacy and security are also important considerations. Big-data analysis of the biological information obtained from various types of skin-mountable devices would be an interesting future research direction.

DISCLOSURE STATEMENT

The authors are not aware of any affiliations, memberships, funding, or financial holdings that might be perceived as affecting the objectivity of this review.

ACKNOWLEDGMENTS

C.H.L is grateful for support from Eli Lilly and Company (F.00120802.02.013), the Ralph W. and Grace M. Showalter Research Trust (F.00120802.02.012), and the Weldon School of Biomedical Engineering and the School of Mechanical Engineering at Purdue University.

LITERATURE CITED

1. Wang S, Oh JY, Xu J, Tran H, Bao Z. 2018. Skin-inspired electronics: an emerging paradigm. *Acc. Chem. Res.* 51:1033–45
2. Lee H, Song C, Baik S, Kim D, Hyeon T, Kim DH. 2018. Device-assisted transdermal drug delivery. *Adv. Drug Deliv. Rev.* 127:35–45
3. Wang X, Dong L, Zhang H, Yu R, Pan C, Wang ZL. 2015. Recent progress in electronic skin. *Adv. Sci.* 2:1500169
4. Lee CH. 2016. Smart assembly for soft bioelectronics. *IEEE Potentials* 35:9–13
5. Chortos A, Bao Z. 2014. Skin-inspired electronic devices. *Mater. Today* 17:321–31
6. Benight SJ, Wang C, Tok JBH, Bao Z. 2013. Stretchable and self-healing polymers and devices for electronic skin. *Prog. Polym. Sci.* 38:1961–77
7. Won SM, Song E, Zhao J, Li J, Rivnay J, Rogers JA. 2018. Recent advances in materials, devices, and systems for neural interfaces. *Adv. Mater.* 30:e1800534
8. Choi J, Ghaffari R, Baker LB, Rogers JA. 2018. Skin-interfaced systems for sweat collection and analytics. *Sci. Adv.* 4:eaar3921
9. Heikenfeld J, Jajack A, Rogers J, Gutruf P, Tian L, et al. 2018. Wearable sensors: modalities, challenges, and prospects. *Lab Chip* 18:217–48
10. Miyamoto A, Lee S, Cooray NF, Lee S, Mori M, et al. 2017. Inflammation-free, gas-permeable, lightweight, stretchable on-skin electronics with nanomeshes. *Nat. Nanotechnol.* 12:907–13
11. Lee Y, Kim J, Joo H, Raj MS, Ghaffari R, Kim D-H. 2017. Wearable sensing systems with mechanically soft assemblies of nanoscale materials. *Adv. Mater. Technol.* 2:1700053
12. Dolbashid AS, Mokhtar MS, Muhamad F, Ibrahim F. 2018. Potential applications of human artificial skin and electronic skin (e-skin): a review. *Bioinspired Biomim. Nanobiomater.* 7:53–64
13. Kim DH, Lu N, Ma R, Kim YS, Kim RH, et al. 2011. Epidermal electronics. *Science* 333:838–43
14. Millington PF, Wilkinson R. 2009. *Skin*. Cambridge, UK: Cambridge Univ. Press
15. Lewis T. 1927. *The Blood Vessels of the Human Skin and Their Responses*. London: Shaw & Sons
16. Olesen BW. 1982. Thermal comfort. *Tech. Rev.* 2:3–43
17. Çetingül MP, Herman C. 2010. A heat transfer model of skin tissue for the detection of lesions: sensitivity analysis. *Phys. Med. Biol.* 55:5933
18. Okabe T, Fujimura T, Okajima J, Aiba S, Maruyama S. 2018. Non-invasive measurement of effective thermal conductivity of human skin with a guard-heated thermistor probe. *Int. J. Heat Mass Transfer* 126:625–35
19. Jin H, Abu-Raya YS, Haick H. 2017. Advanced materials for health monitoring with skin-based wearable devices. *Adv. Healthc. Mater.* 6:1700024
20. Mitsubayashi K, Arakawa T. 2016. Cavitas sensors: contact lens type sensors and mouthguard sensors. *Electroanalysis* 28:1170–87
21. Kim J, Lee M, Shim HJ, Ghaffari R, Cho HR, et al. 2014. Stretchable silicon nanoribbon electronics for skin prosthesis. *Nat. Commun.* 5:5747
22. Schwartz G, Tee BCK, Mei J, Appleton AL, Kim DH, et al. 2013. Flexible polymer transistors with high pressure sensitivity for application in electronic skin and health monitoring. *Nat. Commun.* 4:1859
23. Chortos A, Liu J, Bao Z. 2016. Pursuing prosthetic electronic skin. *Nat. Mater.* 15:937–50
24. Han S, Kim J, Won SM, Ma Y, Kang D, et al. 2018. Battery-free, wireless sensors for full-body pressure and temperature mapping. *Sci. Transl. Med.* 10:eaan4950
25. Dagdeviren C, Shi Y, Joe P, Ghaffari R, Balooch G, et al. 2015. Conformal piezoelectric systems for clinical and experimental characterization of soft tissue biomechanics. *Nat. Mater.* 14:728–36
26. Rim YS, Bae SH, Chen H, De Marco N, Yang Y. 2016. Recent progress in materials and devices toward printable and flexible sensors. *Adv. Mater.* 28:4415–40
27. Tee BCK, Chortos A, Dunn RR, Schwartz G, Eason E, Bao Z. 2014. Tunable flexible pressure sensors using microstructured elastomer geometries for intuitive electronics. *Adv. Funct. Mater.* 24:5427–34
28. Nie B, Xing S, Brandt JD, Pan T. 2012. Droplet-based interfacial capacitive sensing. *Lab Chip* 12:1110–18

29. Nie B, Li R, Cao J, Brandt JD, Pan T. 2015. Flexible transparent iontronic film for interfacial capacitive pressure sensing. *Adv. Mater.* 27:Z6055–62
30. Poh MZ, Loddenkemper T, Swenson NC, Goyal S, Madsen JR, Picard RW. Continuous monitoring of electrodermal activity during epileptic seizures using a wearable sensor. In *Proceedings of the 2010 Annual International Conference of the IEEE Engineering in Medicine and Biology Society*, pp. 4415–18. Piscataway, NJ: IEEE
31. Lin CT, Ko LW, Chang MH, Duann JR, Chen JY, et al. 2010. Review of wireless and wearable electroencephalogram systems and brain-computer interfaces—a mini-review. *Gerontology* 56:112–19
32. Mihajlovic V, Grundlehner B, Vullers R, Penders J. 2015. Wearable, wireless EEG solutions in daily life applications: What are we missing? *IEEE J. Biomed. Health Inform.* 19:6–21
33. Hu B, Peng H, Zhao Q, Hu B, Majoe D, et al. 2015. Signal quality assessment model for wearable EEG Sensor on prediction of mental stress. *IEEE Trans. NanoBiosci.* 14:553–61
34. Patel S, Park H, Bonato P, Chan L, Rodgers M. 2012. A review of wearable sensors and systems with application in rehabilitation. *J. Neuroeng. Rehabil.* 9:21
35. Smith SJM. 2005. EEG in the diagnosis, classification, and management of patients with epilepsy. *J. Neurol. Neurosurg. Psychiatry* 76:ii2–7
36. Jung S, Hong S, Kim J, Lee S, Hyeon T, et al. 2015. Wearable fall detector using integrated sensors and energy devices. *Sci. Rep.* 5:17081
37. Chi YM, Jung TP, Cauwenberghs G. 2010. Dry-contact and noncontact biopotential electrodes: methodological review. *IEEE Rev. Biomed. Eng.* 3:106–19
38. Yao S, Zhu Y. 2016. Nanomaterial-enabled dry electrodes for electrophysiological sensing: a review. *JOM* 68:1145–55
39. Gruetzmann A, Hansen S, Muller J. 2007. Novel dry electrodes for ECG monitoring. *Physiol. Meas.* 28:1375–90
40. Searle A, Kirkup L. 2000. A direct comparison of wet, dry and insulating bioelectric recording electrodes. *Physiol. Meas.* 21:271–83
41. Constantinescu G, Jeong JW, Li X, Scott DK, Jang KI, et al. 2016. Epidermal electronics for electromyography: an application to swallowing therapy. *Med. Eng. Phys.* 38:807–12
42. Norton JJS, Lee DS, Lee JW, Lee W, Kwon O, et al. 2015. Soft, curved electrode systems capable of integration on the auricle as a persistent brain–computer interface. *PNAS* 112:3920–25
43. Tai LC, Gao W, Chao M, Bariya M, Ngo QP, et al. 2018. Methylxanthine drug monitoring with wearable sweat sensors. *Adv. Mater.* 30:1707442
44. Anastasova S, Crewther B, Bembnowicz P, Curto V, Ip HM, et al. 2017. A wearable multisensing patch for continuous sweat monitoring. *Biosens. Bioelectron.* 93:139–45
45. Dang W, Manjakkal L, Navaraj WT, Lorenzelli L, Vinciguerra V, Dahiya R. 2018. Stretchable wireless system for sweat pH monitoring. *Biosens. Bioelectron.* 107:192–202
46. McCaul M, Porter A, Barrett R, White P, Stroiescu F, et al. 2018. Wearable platform for real-time monitoring of sodium in sweat. *Chem. Phys. Chem.* 19:1531–36
47. Gao W, Emaminejad S, Nyein HYY, Challa S, Chen K, et al. 2016. Fully integrated wearable sensor arrays for multiplexed in situ perspiration analysis. *Nature* 529:509–14
48. Farrell PM, Rosenstein BJ, White TB, Accurso FJ, Castellani C, et al. 2008. Guidelines for diagnosis of cystic fibrosis in newborns through older adults: Cystic Fibrosis Foundation Consensus Report. *J. Pediatr.* 153:S4–14
49. Elnaggar YSR, El-Refaie WM, El-Massik MA, Abdallah OY. 2014. Lecithin-based nanostructured gels for skin delivery: an update on state of art and recent applications. *J. Control. Release* 180:10–24
50. Choi J, Kang D, Han S, Kim SB, Rogers JA. 2017. Thin, soft, skin-mounted microfluidic networks with capillary bursting valves for chrono-sampling of sweat. *Adv. Healthc. Mater.* 6:1601355
51. Lee H, Song C, Hong YS, Kim MS, Cho HR, et al. 2017. Wearable/disposable sweat-based glucose monitoring device with multistage transdermal drug delivery module. *Sci. Adv.* 3:e1601314
52. Kinnamon D, Ghanta R, Lin KC, Muthukumar S, Prasad S. 2017. Portable biosensor for monitoring cortisol in low-volume perspired human sweat. *Sci. Rep.* 7:13312
53. Liao C, Zhang M, Niu L, Zheng Z, Yan F. 2013. Highly selective and sensitive glucose sensors based on organic electrochemical transistors with graphene-modified gate electrodes. *J. Mater. Chem. B* 1:3820

54. Tang H, Yan F, Lin P, Xu J, Chan HLW. 2011. Highly sensitive glucose biosensors based on organic electrochemical transistors using platinum gate electrodes modified with enzyme and nanomaterials. *Adv. Funct. Mater.* 21:2264–72
55. Kergoat L, Piro B, Simon DT, Pham MC, Noel V, Berggren M. 2014. Detection of glutamate and acetylcholine with organic electrochemical transistors based on conducting polymer/platinum nanoparticle composites. *Adv. Mater.* 26:5658–64
56. Yang K, Wan J, Zhang S, Tian B, Zhang Y, Liu Z. 2012. The influence of surface chemistry and size of nanoscale graphene oxide on photothermal therapy of cancer using ultra-low laser power. *Biomaterials* 33:2206–14
57. Mannoor MS, Tao H, Clayton JD, Sengupta A, Kaplan DL, et al. 2012. Graphene-based wireless bacteria detection on tooth enamel. *Nat. Commun.* 3:763
58. Kang N, Lin F, Zhao W, Lombardi JP, Almihdhar M, et al. 2016. Nanoparticle–nanofibrous membranes as scaffolds for flexible sweat sensors. *ACS Sens.* 1:1060–69
59. Parlak O, Keene ST, Marais A, Curto VF, Salleo A. 2018. Molecularly selective nanoporous membrane-based wearable organic electrochemical device for noninvasive cortisol sensing. *Sci. Adv.* 4:eaar2904
60. Koh A, Kang D, Xue Y, Lee S, Pielak RM, et al. 2016. A soft, wearable microfluidic device for the capture, storage, and colorimetric sensing of sweat. *Sci. Transl. Med.* 8:366ra165
61. Curto VF, Fay C, Coyle S, Byrne R, O'Toole C, et al. 2012. Real-time sweat pH monitoring based on a wearable chemical barcode micro-fluidic platform incorporating ionic liquids. *Sens. Actuators B* 171/172:1327–34
62. Oncescu V, O'Dell D, Erickson D. 2013. Smartphone based health accessory for colorimetric detection of biomarkers in sweat and saliva. *Lab Chip* 13:3232–38
63. Shen L, Hagen JA, Papautsky I. 2012. Point-of-care colorimetric detection with a smartphone. *Lab Chip* 12:4240–43
64. Castano LM, Flatau AB. 2014. Smart fabric sensors and e-textile technologies: a review. *Smart Mater. Struct.* 23:053001
65. Windmiller JR, Bandodkar AJ, Parkhomovsky S, Wang J. 2012. Stamp transfer electrodes for electrochemical sensing on non-planar and oversized surfaces. *Analyst* 137:1570–75
66. Bujes-Garrido J, Arcos-Martínez MJ. 2017. Development of a wearable electrochemical sensor for voltammetric determination of chloride ions. *Sens. Actuators B* 240:224–28
67. Mishra RK, Martín A, Nakagawa T, Barfidokht A, Lu X, et al. 2018. Detection of vapor-phase organophosphate threats using wearable conformable integrated epidermal and textile wireless biosensor systems. *Biosens. Bioelectron.* 101:227–34
68. Gualandi I, Marzocchi M, Achilli A, Cavedale D, Bonfiglio A, Fraboni B. 2016. Textile organic electrochemical transistors as a platform for wearable biosensors. *Sci. Rep.* 6:33637
69. Zhou G, Byun JH, Oh Y, Jung BM, Cha HJ, et al. 2017. Highly sensitive wearable textile-based humidity sensor made of high-strength, single-walled carbon nanotube/poly(vinyl alcohol) filaments. *ACS Appl. Mater. Interfaces* 9:4788–97
70. Bandodkar AJ, Jia W, Yardimci C, Wang X, Ramirez J, Wang J. 2015. Tattoo-based noninvasive glucose monitoring: a proof-of-concept study. *Anal. Chem.* 87:394–98
71. Emaminejad S, Gao W, Wu E, Davies ZA, Yin Yin Nyein H, et al. 2017. Autonomous sweat extraction and analysis applied to cystic fibrosis and glucose monitoring using a fully integrated wearable platform. *PNAS* 114:4625–30
72. Liu Y, Pharr M, Salvatore GA. 2017. Lab-on-skin: a review of flexible and stretchable electronics for wearable health monitoring. *ACS Nano* 11:9614–35
73. Pang C, Bae W-G, Kim HN, Suh K-Y. 2012. Wearable skin sensors for in vitro diagnostics. *SPIE Newsroom*, Dec. 3. **http://spie.org/newsroom/4554-wearable-skin-sensors-for-in-vitro-diagnostics?SSO=1**
74. Choi S, Lee H, Ghaffari R, Hyeon T, Kim DH. 2016. Recent advances in flexible and stretchable bioelectronic devices integrated with nanomaterials. *Adv. Mater.* 28:4203–18

75. Hamid S, Hayek R. 2008. Role of electrical stimulation for rehabilitation and regeneration after spinal cord injury: an overview. *Eur. Spine J.* 17:1256–69
76. Malešević NM, Maneski LZP, Ilić V, Jorgovanović N, Bijelić G, et al. 2012. A multi-pad electrode based functional electrical stimulation system for restoration of grasp. *J. Neuroeng. Rehabil.* 9:66
77. Micera S, Keller T, Lawrence M, Morari M, Popovic D. 2010. Wearable neural prostheses. *IEEE Eng. Med. Biol. Mag.* 29:64–69
78. Heller BW, Clarke AJ, Good TR, Healey TJ, Nair S, et al. 2013. Automated setup of functional electrical stimulation for drop foot using a novel 64 channel prototype stimulator and electrode array: results from a gait-lab based study. *Med. Eng. Phys.* 35:74–81
79. Choi S, Park J, Hyun W, Kim J, Kim J, et al. 2015. Stretchable heater using ligand-exchanged silver nanowire nanocomposite for wearable articular thermotherapy. *ACS Nano* 9:6626–33
80. Loeser RF, Goldring SR, Scanzello CR, Goldring MB. 2012. Osteoarthritis: a disease of the joint as an organ. *Arthritis Rheum.* 64:1697–707
81. Maghsoudipour M, Moghimi S, Dehghaan F, Rahimpanah A. 2008. Association of occupational and non-occupational risk factors with the prevalence of work related carpal tunnel syndrome. *J. Occup. Rehabil.* 18:152–66
82. Yang K, Freeman C, Torah R, Beeby S, Tudor J. 2014. Screen printed fabric electrode array for wearable functional electrical stimulation. *Sens. Actuators A* 213:108–15
83. Xu B, Akhtar A, Liu Y, Chen H, Yeo WH, et al. 2016. An epidermal stimulation and sensing platform for sensorimotor prosthetic control, management of lower back exertion, and electrical muscle activation. *Adv. Mater.* 28:4462–71
84. Jang NS, Kim KH, Ha SH, Jung SH, Lee HM, Kim JM. 2017. Simple approach to high-performance stretchable heaters based on Kirigami patterning of conductive paper for wearable thermotherapy applications. *ACS Appl. Mater. Interfaces* 9:19612–21
85. DeMuth PC, Li AV, Abbink P, Liu J, Li H, et al. 2013. Vaccine delivery with microneedle skin patches in nonhuman primates. *Nat. Biotechnol.* 31:1082–85
86. Prausnitz MR, Langer R. 2008. Transdermal drug delivery. *Nat. Biotechnol.* 26:1261–68
87. Di J, Yao S, Ye Y, Cui Z, Yu J, et al. 2015. Stretch-triggered drug delivery from wearable elastomer films containing therapeutic depots. *ACS Nano* 9:9407–15
88. Kim YC, Park JH, Prausnitz MR. 2012. Microneedles for drug and vaccine delivery. *Adv. Drug Deliv. Rev.* 64:1547–68
89. Mitragotri S, Blankschtein D, Langer R. 1995. Ultrasound-mediated transdermal protein delivery. *Science* 269:850–53
90. Shin J, Shin K, Lee H, Nam JB, Jung JE, et al. 2010. Non-invasive transdermal delivery route using electrostatically interactive biocompatible nanocapsules. *Adv. Mater.* 22:739–43
91. Sullivan SP, Koutsonanos DG, Del Pilar Martin M, Lee JW, Zarnitsyn V, et al. 2010. Dissolving polymer microneedle patches for influenza vaccination. *Nat. Med.* 16:915–20
92. Yu J, Zhang Y, Ye Y, DiSanto R, Sun W, et al. 2015. Microneedle-array patches loaded with hypoxia-sensitive vesicles provide fast glucose-responsive insulin delivery. *PNAS* 112:8260–65
93. Vadlapatla R, Wong EY, Gayakwad SG. 2017. Electronic drug delivery systems: an overview. *J. Drug Deliv. Sci. Technol.* 41:359–66
94. Lee H, Choi TK, Lee YB, Cho HR, Ghaffari R, et al. 2016. A graphene-based electrochemical device with thermoresponsive microneedles for diabetes monitoring and therapy. *Nat. Nanotechnol.* 11:566–72
95. Lee JW, Park JH, Prausnitz MR. 2008. Dissolving microneedles for transdermal drug delivery. *Biomaterials* 29:2113–24
96. Ita K. 2017. Dissolving microneedles for transdermal drug delivery: advances and challenges. *Biomed. Pharmacother.* 93:1116–27
97. Kim J, Son D, Lee M, Song C, Song JK, et al. 2016. A wearable multiplexed silicon nonvolatile memory array using nanocrystal charge confinement. *Sci. Adv.* 2:e1501101
98. Choi MK, Park OK, Choi C, Qiao S, Ghaffari R, et al. 2016. Cephalopod-inspired miniaturized suction cups for smart medical skin. *Adv. Healthc. Mater.* 5:80–87

99. Ogawa Y, Kato K, Miyake T, Nagamine K, Ofuji T, et al. 2015. Organic transdermal iontophoresis patch with built-in biofuel cell. *Adv. Healthc. Mater.* 4:506–10
100. Son D, Lee J, Qiao S, Ghaffari R, Kim J, et al. 2014. Multifunctional wearable devices for diagnosis and therapy of movement disorders. *Nat. Nanotechnol.* 9:397–404
101. Lee JE, Lee N, Kim T, Kim J, Hyeon T. 2011. Multifunctional mesoporous silica nanocomposite nanoparticles for theranostic applications. *Acc. Chem. Res.* 44:893–902
102. Peer D, Karp JM, Hong S, Farokhzad OC, Margalit R, Langer R. 2007. Nanocarriers as an emerging platform for cancer therapy. *Nat. Nanotechnol.* 2:751–60
103. Herbert R, Kim JH, Kim YS, Lee H, Yeo WH. 2018. Soft material–enabled, flexible hybrid electronics for medicine, healthcare, and human–machine interfaces. *Materials* 11:E187
104. Wagner S, Bauer S. 2012. Materials for stretchable electronics. *MRS Bull.* 37:207–13
105. Gonzalez M, Vandevelde B, Christiaens W, Hsu YY, Iker F, et al. 2011. Design and implementation of flexible and stretchable systems. *Microelectron. Reliab.* 51:1069–76
106. Sterken T, Vanfleteren J, Torfs T, de Beeck MO, Bossuyt F, Van Hoof C. 2011. Ultra-thin chip package (UTCP) and stretchable circuit technologies for wearable ECG system. In *Proceedings of the 2011 Annual International Conference of the IEEE Engineering in Medicine and Biology Society*, pp. 6886–89. Piscataway, NJ: IEEE
107. Kaltenbrunner M, Sekitani T, Reeder J, Yokota T, Kuribara K, et al. 2013. An ultra-lightweight design for imperceptible plastic electronics. *Nature* 499:458–63
108. White MS, Kaltenbrunner M, Głowacki ED, Gutnichenko K, Kettlgruber G, et al. 2013. Ultrathin, highly flexible and stretchable PLEDs. *Nat. Photonics* 7:811–16
109. Xu S, Zhang Y, Jia L, Mathewson KE, Jang KI, et al. 2014. Soft microfluidic assemblies of sensors, circuits, and radios for the skin. *Science* 344:70–74
110. Lee CH, Ma Y, Jang KI, Banks A, Pan T, et al. 2015. Soft core/shell packages for stretchable electronics. *Adv. Funct. Mater.* 25:3698–704
111. Lipomi DJ, Vosgueritchian M, Tee BCK, Hellstrom SL, Lee JA, et al. 2011. Skin-like pressure and strain sensors based on transparent elastic films of carbon nanotubes. *Nat. Nanotechnol.* 6:788–92
112. Choong CL, Shim MB, Lee BS, Jeon S, Ko DS, et al. 2014. Highly stretchable resistive pressure sensors using a conductive elastomeric composite on a micropyramid array. *Adv. Mater.* 26:3451–58
113. Gong S, Schwalb W, Wang Y, Chen Y, Tang Y, et al. 2014. A wearable and highly sensitive pressure sensor with ultrathin gold nanowires. *Nat. Commun.* 5:3132
114. Yamada T, Hayamizu Y, Yamamoto Y, Yomogida Y, Izadi-Najafabadi A, et al. 2011. A stretchable carbon nanotube strain sensor for human-motion detection. *Nat. Nanotechnol.* 6:296–301
115. Pang C, Lee GY, Kim TI, Kim SM, Kim HN, et al. 2012. A flexible and highly sensitive strain-gauge sensor using reversible interlocking of nanofibres. *Nat. Mater.* 11:795–801
116. Amjadi M, Pichitpajongkit A, Lee S, Ryu S, Park I. 2014. Highly stretchable and sensitive strain sensor based on silver nanowire–elastomer nanocomposite. *ACS Nano* 8:5154–63
117. Boland CS, Khan U, Backes C, O'Neill A, McCauley J, et al. 2014. Sensitive, high-strain, high-rate bodily motion sensors based on graphene–rubber composites. *ACS Nano* 8:8819–30
118. Kenry, Yeo JC, Yu J, Shang M, Loh KP, Lim CT. 2016. Highly flexible graphene oxide nanosuspension liquid–based microfluidic tactile sensor. *Small* 12:1593–604
119. Jung T, Yang S. 2015. Highly stable liquid metal–based pressure sensor integrated with a microfluidic channel. *Sensors* 15:11823–35
120. Chossat JB, Park YL, Wood RJ, Duchaine V. 2013. A soft strain sensor based on ionic and metal liquids. *IEEE Sens. J.* 13:3405–14
121. Kim SY, Park S, Park HW, Park DH, Jeong Y, Kim DH. 2015. Highly sensitive and multimodal all-carbon skin sensors capable of simultaneously detecting tactile and biological stimuli. *Adv. Mater.* 27:4178–85
122. Gerratt AP, Michaud HO, Lacour SP. 2015. Elastomeric electronic skin for prosthetic tactile sensation. *Adv. Funct. Mater.* 25:2287–95
123. Wang J, Jiu J, Nogi M, Sugahara T, Nagao S, et al. 2015. A highly sensitive and flexible pressure sensor with electrodes and elastomeric interlayer containing silver nanowires. *Nanoscale* 7:2926–32

124. Li R, Nie B, Digiglio P, Pan T. 2014. Microflotronics: a flexible, transparent, pressure-sensitive microfluidic film. *Adv. Funct. Mater.* 24:6195–203
125. Cohen DJ, Mitra D, Peterson K, Maharbiz MM. 2012. A highly elastic, capacitive strain gauge based on percolating nanotube networks. *Nano Lett.* 12:1821–25
126. Gullapalli H, Vemuru VSM, Kumar A, Botello-Mendez A, Vajtai R, et al. 2010. Flexible piezoelectric ZnO–paper nanocomposite strain sensor. *Small* 6:1641–46
127. Dagdeviren C, Su Y, Joe P, Yona R, Liu Y, et al. 2014. Conformable amplified lead zirconate titanate sensors with enhanced piezoelectric response for cutaneous pressure monitoring. *Nat. Commun.* 5:4496
128. Persano L, Dagdeviren C, Su Y, Zhang Y, Girardo S, et al. 2013. High performance piezoelectric devices based on aligned arrays of nanofibers of poly(vinylidenefluoride-*co*-trifluoroethylene). *Nat. Commun.* 4:1633
129. Nie B, Li R, Brandt JD, Pan T. 2014. Iontronic microdroplet array for flexible ultrasensitive tactile sensing. *Lab Chip* 14:1107–16
130. Nie B, Li R, Brandt JD, Pan T. 2014. Microfluidic tactile sensors for three-dimensional contact force measurements. *Lab Chip* 14:4344–53
131. Mitsubayashi K, Wakabayashi Y, Murotomi D, Yamada T, Kawase T, et al. 2003. Wearable and flexible oxygen sensor for transcutaneous oxygen monitoring. *Sens. Actuators B* 95:373–77
132. Yang YL, Chuang MC, Lou SL, Wang J. 2010. Thick-film textile–based amperometric sensors and biosensors. *Analyst* 135:1230–34
133. Xuan X, Yoon HS, Park JY. 2018. A wearable electrochemical glucose sensor based on simple and low-cost fabrication supported micro-patterned reduced graphene oxide nanocomposite electrode on flexible substrate. *Biosens. Bioelectron.* 109:75–82
134. Martín A, Kim J, Kurniawan JF, Sempionatto JR, Moreto JR, et al. 2017. Epidermal microfluidic electrochemical detection system: enhanced sweat sampling and metabolite detection. *ACS Sens.* 2:1860–68
135. Schazmann B, Morris D, Slater C, Beirne S, Fay C, et al. 2010. A wearable electrochemical sensor for the real-time measurement of sweat sodium concentration. *Anal. Methods* 2:342–48
136. Gonzalo-Ruiz J, Mas R, de Haro C, Cabruja E, Camero R, et al. 2009. Early determination of cystic fibrosis by electrochemical chloride quantification in sweat. *Biosens. Bioelectron.* 24:1788–91
137. Bandodkar AJ, Hung VWS, Jia W, Valdés-Ramírez G, Windmiller JR, et al. 2013. Tattoo-based potentiometric ion-selective sensors for epidermal pH monitoring. *Analyst* 138:123–28
138. Guinovart T, Bandodkar AJ, Windmiller JR, Andrade FJ, Wang J. 2013. A potentiometric tattoo sensor for monitoring ammonium in sweat. *Analyst* 138:7031–38
139. Bandodkar AJ, Molinnus D, Mirza O, Guinovart T, Windmiller JR, et al. 2014. Epidermal tattoo potentiometric sodium sensors with wireless signal transduction for continuous non-invasive sweat monitoring. *Biosens. Bioelectron.* 54:603–9
140. Khodagholy D, Curto VF, Fraser KJ, Gurfinkel M, Byrne R, et al. 2012. Organic electrochemical transistor incorporating an ionogel as a solid state electrolyte for lactate sensing. *J. Mater. Chem.* 22:4440–43
141. Jessen C. 2000. *Temperature Regulation in Humans and Other Mammals*. Berlin: Springer
142. Mukamal R, Harrison DA. 2016. *Facts About Tears*. San Francisco: Am. Acad. Ophthalmol. **https://www.aao.org/eye-health/tips-prevention/facts-about-tears**
143. Baker LB. 2017. Sweating rate and sweat sodium concentration in athletes: a review of methodology and intra/interindividual variability. *Sports Med.* 47:111–28
144. Farandos NM, Yetisen AK, Monteiro MJ, Lowe CR, Yun SH. 2015. Contact lens sensors in ocular diagnostics. *Adv. Healthc. Mater.* 4:792–810
145. Autran de Morais HA, DiBartola SB, ed. 2012. *Advances in Fluid, Electrolyte, and Acid-Base Disorders in Small Animal Practice*. Columbus, OH: Elsevier Saunders. 4th ed.
146. Stahl U, Willcox M, Stapleton F. 2012. Osmolality and tear film dynamics. *Clin. Exp. Optom.* 95:3–11
147. Abelson MB, Udell IJ, Weston JH. 1981. Normal human tear pH by direct measurement. *Arch. Ophthalmol.* 99:301
148. Badugu R, Lakowicz JR, Geddes CD. 2004. Ophthalmic glucose monitoring using disposable contact lenses—a review. *J. Fluoresc.* 14:617–33

Annual Review
of Biomedical
Engineering

Volume 21, 2019

Contents

Errata

An online log of corrections to *Annual Review of Biomedical Engineering* articles may be found at http://www.annualreviews.org/errata/bioeng